International Journal of Marine Engineering Innovation and Research, Vol. 11(1), Mar. 2026. 67-76
(pISSN: 2541-5972, eISSN: 2548-1479)

Period of Efficient Underwater Hull Cleaning

Rifqi Al Baihaqi Wijaya[1*], Achmad Baidowi [2], Sunarsih [3]
(Received: 15 January 2026 / Revised: 28 January 2026 / Accepted: 2 February 2026 / Available Online: 7 March 2026)

***Abstract*—** Biofouling is a collection of unwanted living organisms on surfaces submerged in water. Biofouling is a complex occurrence caused by various physical and environmental factors that can be overcome by regular hull cleaning. The main purpose of underwater hull cleaning is to remove dirt and restore propulsion efficiency. Another benefit of hull cleaning against biofouling is to restore or rejuvenate the effectiveness of antifouling paint. This study aims to determine the extent of the effect of periodic underwater hull cleaning, with results used to determine the most efficient time interval for performing periodic hull cleaning and the percentage of fuel that can be saved by performing periodic underwater cleaning. The methods used in this study included identifying biofouling growth through flat-plate experiments immersed in the waters of the Madura Strait and modeling surface roughness growth using regression simulations based on Computational Fluid Dynamics (CFD) on a three-dimensional tanker model. Simulations were conducted with speed variations of 10, 12, 14, and 16 knots, and biofouling growth periods of 7, 12, 18, and 24 months. The study's results show that biofouling increases ship resistance by an average of 2-3% per month compared to ships with clean hulls. Analysis of underwater hull-cleaning scenarios shows that cleaning at 18 months results in the lowest fuel consumption across all speed variations tested. At a speed of 10 knots, fuel savings reached 5.7% or 54.93 tons, at 12 knots 3.3% or 59.65 tons, at 14 knots 2.7% or 101.76 tons, and at 16 knots 9.3% or 1421.21 tons compared to ships without hull cleaning. In conclusion, the most efficient underwater hull cleaning period is every 18 months after sailing.

Keywords—Biofouling, Underwater Hull Cleaning, Resistance, Computational Fluid Dynamics

[*]*Corresponding Author: rifqialbaihaqiw@gmail.com*

I. INTRODUCTION

Shipping is a critical mode of transportation, commensurate with the increasing importance and dependence on sea transportation. However, technological advances in marine technology have brought several problems for the industry, including increased fuel consumption that damages the environment and reduces company revenues [1]. The attachment and growth of living organisms on surfaces exposed to aquatic environments is defined as fouling. Biofouling communities form through colonization of new surfaces, with succession through several stages [2]. Biofouling on ship hulls in contact with seawater is the leading cause of several technical and economic problems in the shipping industry [3].

Ships released 870 million tonnes of CO2 in 2007, or 2.7% of all CO2 emissions that year, even though shipping is marginally greener than other forms of transportation [4]. According to resistance theory, biofouling on ships' hulls and keels can increase fuel consumption [5]. Fouling on the hull below the waterline can also mean increased fuel costs [6]. Biofouling attached to the hull of a ship can reduce a ship's power by up to 86% at cruising speed. Even relatively light fouling caused by diatom algae can result in a 10% to 16% reduction [7]. Fuel consumption can increase by up to 40% unless preventive measures are taken to prevent fouling. To minimize these [8]. Factors to consider when selecting an antifouling system include expected dry-docking period, ship speed, ship operating profile, ship type, and legal requirements [8].

The primary purpose of cleaning a ship's underwater hull is to remove dirt and restore propulsion efficiency. Another benefit of cleaning a ship's hull to reduce biofouling is to restore or rejuvenate the effectiveness of anti-fouling paint [9]. There are two primary methods for restoring ship performance through hull cleaning: underwater cleaning, in which staff wash the hull surface, and dry-docking cleaning. On the other hand, the ship is securely anchored at the dock [10]. However, the main drawbacks of this method are the high docking and paint repair costs, long docking cycles, and severe pollution. Another reason this method is complicated is the difficulty of coordinating ship sailing schedules [11].

This research highlights the optimal time to clean the underwater hull area and how biofouling affects fuel consumption efficiency at different times, with underwater hull cleaning simulated using Computational Fluid Dynamics (CFD). The results can be used as a reference for ship maintenance, especially for the underwater hull area.

II. METHOD

A. Biofouling Growth Identification

At this stage, biofouling growth was identified through experiments using flat plates measuring 10 cm long x 10 cm wide x 0.3 cm high, which were immersed in water from the Madura Strait [12]. After collecting data from the flat plate experiments, a simulation was conducted with Fine Marine to determine the roughness resulting from biofouling attachment. After obtaining data from the flat-plate simulation (see Table 1.), regression analysis was performed on the simulation results to estimate the increase in roughness due to biofouling attachment. The regression results showed the

Rifqi Al Baihaqi Wijaya, Department of Marine Engineering, Faculty of Marine Technology, Institut Teknologi Sepuluh Nopember, Surabaya, Indonesia. Email: rifqialbaihaqiw@gmail.com
Achmad Baidowi, Department of Marine Engineering, Faculty of Marine Technology, Institut Teknologi Sepuluh Nopember, Surabaya, Indonesia. Email: achmad.baidowi@its.ac.id
Sunarsih, Department of Marine Engineering, Faculty of Marine Technology, Institut Teknologi Sepuluh Nopember, Surabaya, Indonesia. Email: sunarsih@its.ac.id

amount of roughness at 7, 12, 18, and 24 months; see Table 2.

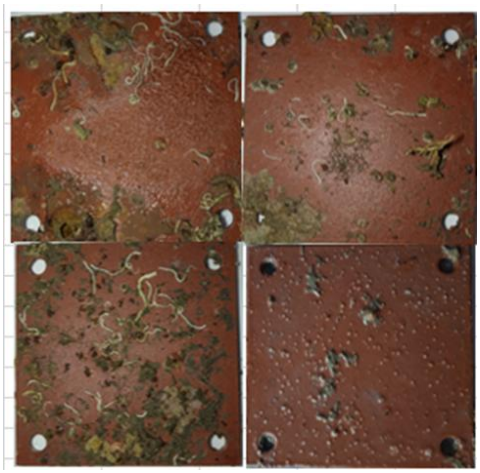

Figure. 1. Fouling conditions on test specimens [11]

TABLE 1.
SIMULATION RESULTS OF FLAT PLATE

Computation name	Froude	Month 7 Resistance (Kn)	Month 8 Resistance (Kn)	Month 9 Resistance (Kn)	Month 12 Resistance (Kn)
biokec01	0.1	0.00302885	0.00322881	0.00326405	0.00359498
biokec03	0.3	0.00302635	0.00322689	0.00326264	0.00359251
biokec05	0.5	0.00302544	0.00322615	0.00326209	0.00359146
biokec07	0.7	0.00302502	0.00322577	0.0032618	0.00359087
biokec09	0.9	0.00302473	0.00322556	0.00326163	0.00359051
biokec11	1.1	0.00302451	0.00322542	0.00326152	0.00359028
biokec13	1.3	0.00302425	0.00322532	0.00326143	0.0035901
AVERAGE		0.003025593	0.003226274	0.003262166	0.00359153

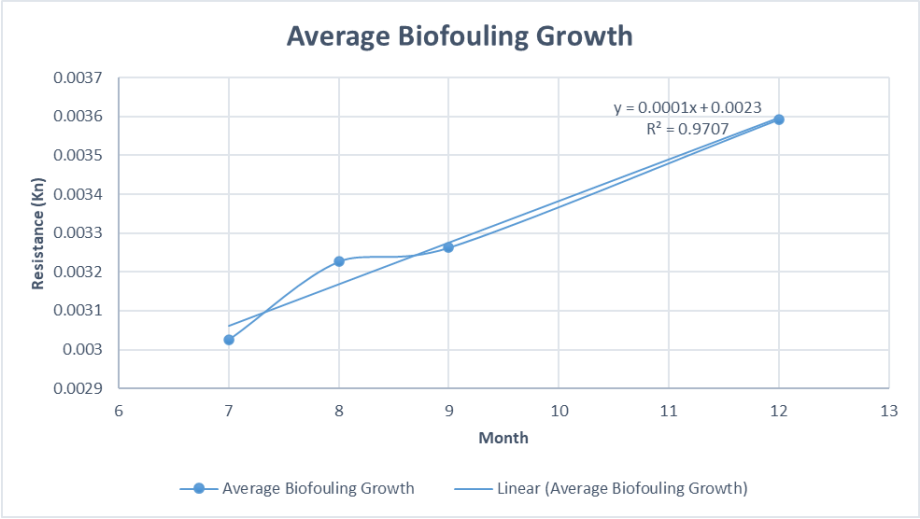

Figure. 2. Average biofouling growth chart

Based on the results of the biofouling growth experiment, the biofouling growth rate was modeled using the available growth regression graph. In this experiment, the regression equation obtained was:

$$Y = 0.0001x + 0.0023 \quad (1)$$

From the following equation, biofouling growth can be predicted at 7, 12, 18, and 24 months as follows:

TABLE 2.
PREDICTION OF BIOFOULING GROWTH RATE

Month	Roughness (mm)
7	0.00306
12	0.00360
18	0.00424
24	0.00488

B. Data Collection and Modeling

This study This study uses a 3-dimensional model of a tanker, generated in Maxsurf software, based on simulation conditions, as shown in Figure 2. The model has evenly distributed hull conditions throughout the underwater area.

Figure. 3. 3D model for regular roughness simulation

C. Governing Equation

The incompressible Reynolds-averaged Navier-Stokes (RANS) equations are solved by the FINETM/Marine CFD code [13]. The conservation equations for mass, momentum, and volume fraction in a multi-phase continuum for incompressible viscous fluid flow under isothermal circumstances can be expressed in Cartesian coordinates as equations (2-4) [14] using the generic form of Gauss's theorem.

$$\frac{\partial}{\partial_u}\int_v \rho\, dV + \int_s \rho(U - U_d).\, n\, dS = 0 \tag{2}$$

$$\frac{\partial}{\partial_u}\int_v \rho U_i\, dV + \int_s \rho U_i(U - U_d).n\, dS = \int_s \left(\tau_{ij}I_j - Pl_i\right).n\, dS + \int_s \rho g_i\, dV \tag{3}$$

$$\frac{\partial}{\partial_u}\int_v c_i\, dV + \int_s c_i(U - U_d).\, n\, dS = 0 \tag{4}$$

A closed surface S, flowing at velocity Ud, and a unit normal vector n pointing outward constitute the domain under examination or control volume, V, in Equations (2-3). The velocity and pressure fields are denoted by the letters U and p, respectively. Moreover, the components of the gravity vector and the viscous stress tensor are represented by gi and τij, respectively. In addition, Ij is a vector with one missing component—the j component, which equals 1. The volume fraction of fluid I, or Ci, is used to determine whether fluid is present (Ci = 1) or not (Ci = 0). (i). This work used the two-equation k-ω SST turbulence model (where SST stands for shear stress transport) [14]. The k-ω model for the outer area and the k-ω model for the inner boundary layer are combined in this turbulence model. The following are the transport equations for the k-ω SST model:

$$\frac{\partial}{\partial_t}(\rho k) + \frac{\partial}{\partial_{xi}}\left(\Gamma_k \frac{\partial_k}{\partial_{xj}}\right) + G_k - Y_k \tag{5}$$

$$\frac{\partial}{\partial_t}(\rho\omega) + \frac{\partial}{\partial_{xi}}(\rho\omega u_i) = \frac{\partial}{\partial_{xi}}\left(\Gamma_\omega \frac{\partial_\omega}{\partial_{xi}}\right) + G_\omega - Y_\omega + D_\omega \tag{6}$$

Equations (5-6) show that Gk is the turbulent kinetic energy generated by the average velocity gradient, Gω is the turbulent kinetic energy generated by ω, and Yk and Yω are the turbulence-induced decay of k and ω, respectively. Additionally, Dω is the cross-diffusion term, and Γk and Γω are the effective diffusivities of k and ω, respectively. The onset and extent of flow separation can be accurately predicted using this turbulence model [15].

By monitoring the volume fraction of each phase in a control cell, the Volume of Fluid (VOF) method is a numerical methodology for capturing the interface between two fluid phases [16]. Free surface flow is simulated using the volume of fluid (VOF) model. The

position of the water surface is implicitly determined using the conservation equation for the water volume fraction [17]. The volume fraction is used to determine the water-to-air interface [18].

The water volume fraction in each cell is represented by a scalar field, α, defined via the VOF method. When the cell is filled with water, this field's value is 1, and when it is filled with air, it is 0. The α values of the cells at the interface range from 0 to 1. Using α as the weight and interpolating between water and air, the fluid characteristics are defined as follows [19]:

$$\rho = \alpha\rho_{water} + (1 - \alpha)\rho_{air} \quad (7)$$

$$\mu = \alpha\mu_{water} + (1 - \alpha)\mu_{air} \quad (8)$$

The VoF field is advected by the velocity field U, as in the following equation:

$$\frac{\partial_a}{\partial_t} + \nabla(Ua) = 0 \quad (9)$$

The VoF two-phase solver used in the ISIS-CFD flow solver is represented by equations (8–9) [20]. EMN (Equipe Modélization Numüge) developed this solver. This solver creates a spatial discretization of transport equations using the discrete volume method. The face-based approach is expanded to two-dimensional unstructured grids, rotationally symmetric grids, or three-dimensional grids where successive faces constrain non-overlapping control volumes. Moving grids and multi-phase flows can be handled by the flow solver [21].

The momentum conservation equation yields the velocity field. On the other hand, the mass conservation equation, also known as the continuity equation, is transformed into a pressure equation to obtain the pressure field [22]. Additional transport equations for modeled variables in turbulent flow can be discretized and solved using the same techniques as the momentum equation. Conservation equations for each phase volume fraction are used to simulate the incompressible, unmixed flow phase.

D. Geometrical Modeling, Meshing, and boundary conditions

This research uses a 3-dimensional model of the hull of the underwater area. Numerical simulation results from the interpolation of boundary condition values during the calculation, leading to incorrect results and divergence due to unrealistic boundary condition values. Divergence is the opposite of convergence, and in a simulation, the results can be trusted if they reach the convergence value. Convergence can occur if the residual or conservation measure of the fluid characteristics as a whole approaches zero [23]. However, other factors affect the accuracy of numerical simulation results, particularly in CFD simulations, where boundary conditions must be defined to describe the problem and achieve the desired results accurately. Boundary conditions are geometric constraints in numerical simulations [24].

The domain is defined by a box surrounding the ship, with its size determined by the ship's length [25]. Only half of the ship is simulated because of symmetry. As illustrated in Figure 2, the computational domain's boundary conditions are as follows: the entrance is situated 1.5 L upstream of the ship. The outflow is situated 3.0 L behind the vessel. The side wall is situated next to the ship at 1.5 L, where L is entirely at the waterline. The free-flow far-field velocity is used as the boundary condition at the inlet, outlet, and side walls. The boundary conditions are defined at the specified pressure, and the top and bottom walls are situated 1.5 L above and 1 L below the ship, respectively. A wall function with a specific roughness is used to specify the boundary conditions on the hull. Additionally, the simulation solves pitch and heave motions.

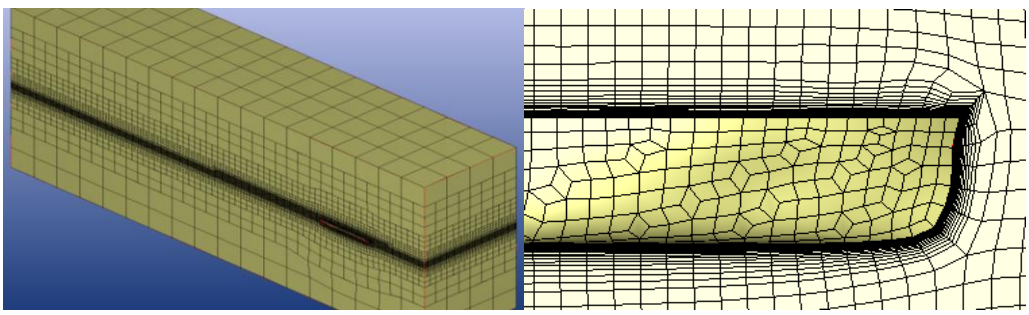

Figure. 4. Computational domain containing the hull form mesh (right) and the ship model (left)

E. Pre-Processor Simulation

After modeling and meshing the ship hull plate, the next step is to enter the preprocessor and determine the boundary conditions on the ship hull. Several parameters Froude numbers. The simulation was carried out using a straightforward method. The simulation model used is must be determined in the FINE Marine software. The flow turbulence model used in this study is the K-Omega (SST-Menter) model. The simulation size and speed parameters are required to obtain the Reynolds and shown in Table 3.

TABLE 3.
SETTING UP SIMULATION

Parameters	Properties
System	Steady state
Model	SST K-omega
Method	Simple
Velocity Inlet (knot)	10, 12, 14, 16

F. Grid independence tests

Tests were carried out to ensure the numerical results satisfied the grid-independence requirements, identify the optimal grid size (number of cells), and assess convergence of the numerical solutions. By adding more cells to the simulation, the total ship resistance coefficient (Cr) was computed in these tests. There were about twice as many cells in the last simulation as in the first two. The percentage of error was computed to measure the difference in Cr between the most recent and previous simulations. The results are summarised in Table 3 and shown in Figure 5. From Table 3. And Figure 5. It can be concluded that meshing values of more than 2 million result in simulation resistance differences of less than 3%. Therefore, it was decided that the meshing value or number of cells used would be ±2 million cells/grid. The biofouling area ratio is the ratio between the wet area containing biofouling and the total wet area of the ship's hull.

TABLE 4.
GRID INDEPENDENCE TESTS

Simulation	Mess/Cell	Resistance (N)	Difference (%)
1	900.650	58.43	0%
2	1.795.250	54.60	6.77%
3	2.331.753	53.48	2.07%
4	2.505.825	53.01	0.89%

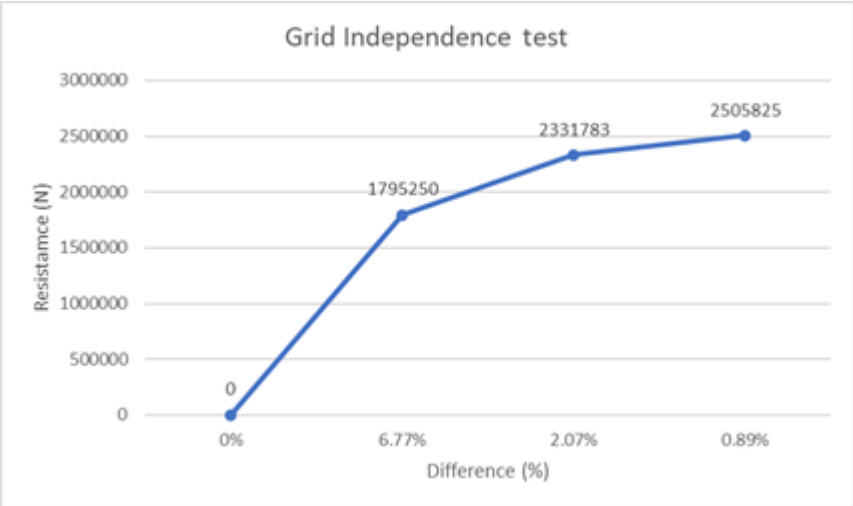

Figure. 5. Grid Independence Test

III. RESULTS AND DISCUSSION

A. General

The Analysis and Discussion chapter is where the data obtained is processed, analyzed, and calculated, then discussed. In accordance with the problem formulation described earlier, this Analysis and Discussion will examine the effect of cleaning the underwater area of a ship's hull. This data analysis presents the results of several simulation variations, including regular roughness models and irregular roughness models with roughness and speed variations of 10, 12, 14, and 16 knots.

B. Analysis of the Efficient Time Period for cleaning the underwater area

1. Analysis of No Fouling hulls with hulls from the 7th period

Figure 6. and Table 5. Show a comparison of clean hull simulation results with hull results in the 7th period above shows an increase in resistance when comparing clean hull conditions with hull conditions in the 7th period, with the most significant increase at a speed of 10 knots with a percentage increase of 2.7% and the lowest increase in resistance at a speed of 14 knots with a percentage increase of 0.6%. Meanwhile, the average increase in resistance in the 7th period is 1.6%.

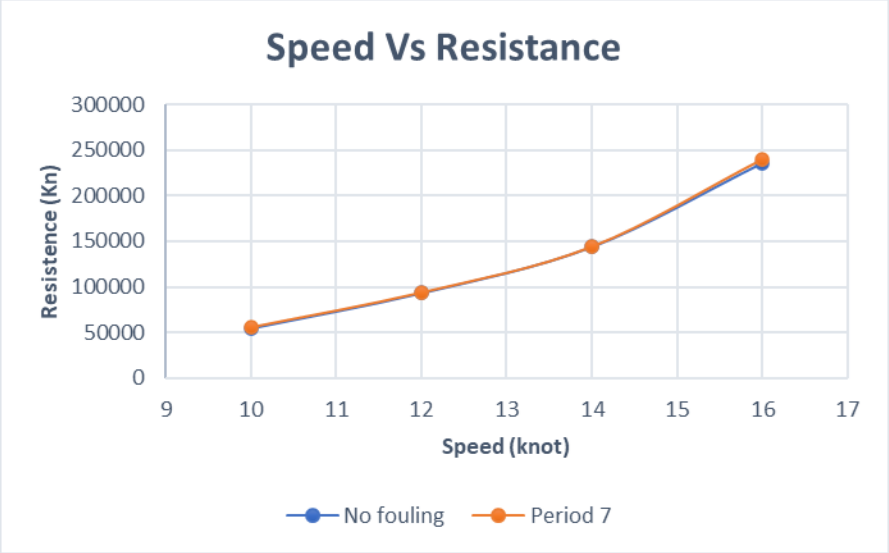

Figure. 6. Comparison chart of No Fouling hull resistance with the 7th period

TABLE 5.
COMPARISON OF NO FOULING BOWL RESISTANCE WITH THE 7TH PERIOD

Speed (Knot)	Speed [m/s]	Froude	Period 7 Resistance (Kn)	No Fouling Resistance (Kn)	Difference (%)
10	5.14	0.161	56104.5	54614.4	2.7%
12	6.17	0.193	94211.5	93150	1.1%
14	7.2	0.226	144422	143626	0.6%
16	8.23	0.258	240117	235161	2.1%
AVERAGE					1.6%

2. Analysis of the hull of the No Fouling ship with the hull of the 12th period ship

Figure 7. and Table 6. Show a comparison of clean hull simulation results with hull results in the 12th period above shows an increase in resistance when comparing clean hull conditions with hull conditions in the 12th period, with the most significant increase at a speed of 10 knots with a percentage increase of 5.2% and the lowest increase in resistance at a speed of 14 knots with a percentage increase of 1.3%. Meanwhile, the average increase in resistance in the 12th period is 3.0%.

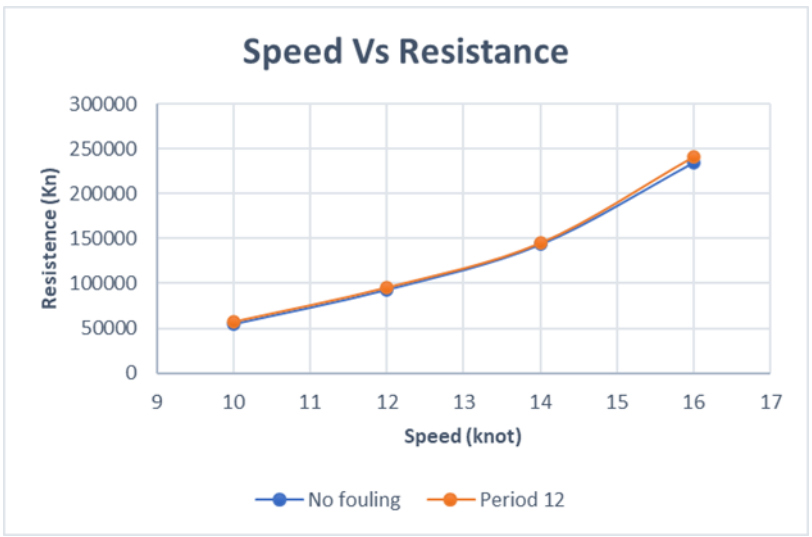

Figure. 7. Comparison chart of fouling-free hull resistance with the 12th period

TABLE 6.
COMPARISON OF NO FOULING BOWL RESISTANCE WITH THE 12TH PERIOD

Speed (Knot)	Speed [m/s]	Froude	Period 12 Resistance (Kn)	No Fouling Resistance (Kn)	Difference (%)
10	5.14	0.161	57634.7	54614.4	5.2%
12	6.17	0.193	95966.8	93150	2.9%
14	7.2	0.226	145486	143626	1.3%
16	8.23	0.258	241597	235161	2.7%
AVERAGE					3.0%

3. Analysis of the hull of the No Fouling ship with the hull of the 18th period ship

Figure 8. and Table 7. Show a comparison of clean hull simulation results with hull results in the 18th period above shows an increase in resistance when comparing clean hull conditions with hull conditions in the 18th period, with the most significant increase at a speed of 10 knots with a percentage increase of 5.4%, while the lowest increase in resistance is at a speed of 14 knots with a percentage increase of 1.6%. Meanwhile, the average increase in resistance in the 18th period is 3.4%.

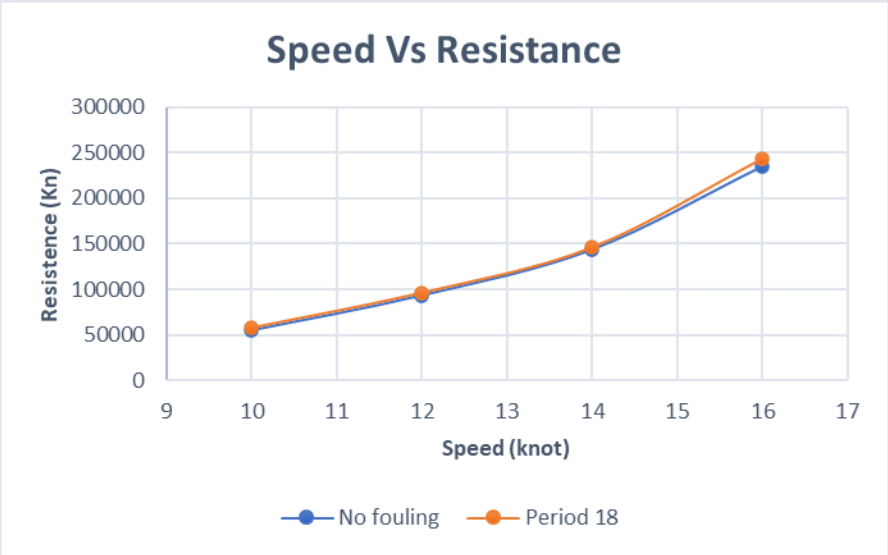

Figure. 8. Comparison chart of fouling-free hull resistance with the 18th period

TABLE 7.
COMPARISON OF NO FOULING BOWL RESISTANCE WITH THE 18TH PERIOD

Speed (Knot)	Speed [m/s]	Froude	Period 18 Resistance (Kn)	No Fouling Resistance (Kn)	Difference (%)
10	5.14	0.161	57713.9	54614.4	5.4%
12	6.17	0.193	96265.5	93150	3.2%
14	7.2	0.226	145992	143626	1.6%
16	8.23	0.258	243296	235161	3.3%
AVERAGE					3.4%

4. Analysis of the hull of the No Fouling ship with the hull of the 24th period ship

Figure 9. and Table 8. Show a comparison of clean hull simulation results with hull results in the 24th period above shows an increase in resistance when comparing clean hull conditions with hull conditions in the 24th period, with the most significant increase at a speed of 10 knots with a percentage increase of 6.3%, while the lowest increase in resistance was at a speed of 14 knots with a percentage increase of 1.8%. Meanwhile, the average increase in resistance in the 24th period is 4.8%.

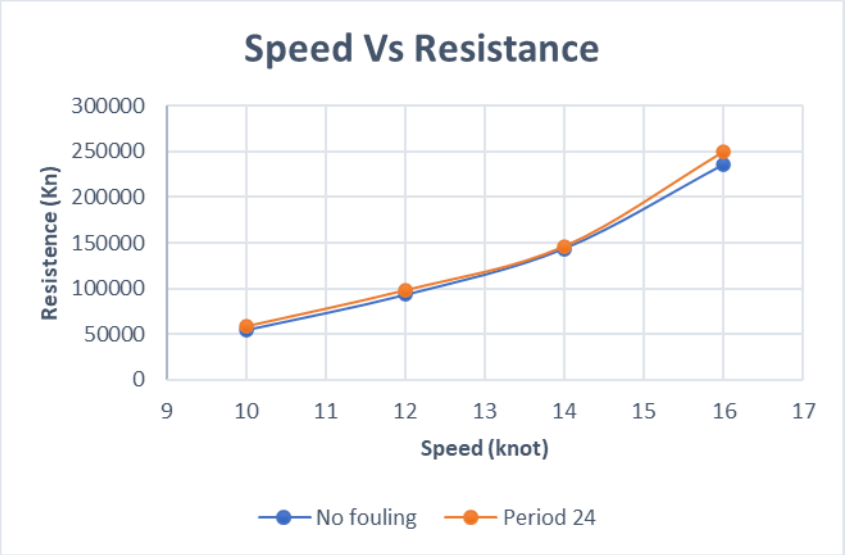

Figure. 9. Comparison chart of fouling-free hull resistance with the 24th period

TABLE 8.
COMPARISON OF NO FOULING BOWL RESISTANCE WITH THE 24TH PERIOD

Speed (Knot)	Speed [m/s]	Froude	Period 24 Resistance (Kn)	No Fouling Resistance (Kn)	Difference (%)
10	5.14	0.161	58315.3	54614.4	6.3%
12	6.17	0.193	98030	93150	5.0%
14	7.2	0.226	146260	143626	1.8%
16	8.23	0.258	250258	235161	6.0%
AVERAGE					4.8%

C. Analysis of Ship Hull Cleaning Timing Determination

The optimal timing for hull cleaning is determined by the increase in fuel consumption and the additional hull-cleaning costs. The sum of the additional fuel consumption and the additional hull cleaning costs must be minimized. In this study, three cleaning scenarios were conducted to find the optimal cost. Namely, cleaning in the 12th, 18th, and 24th months. The fuel consumption increase scenarios with the cleaning scenarios are as follows:

1. Hull Cleaning Time Scenario and Additional Fuel Consumption at 10 Knots

Table 9 presents the three scenarios at 10 knots. The results indicate that the lowest fuel consumption is achieved when hull cleaning is carried out in month 18, with a total additional fuel consumption of 26.5 tons over 24 months. The cumulative fuel consumption for this scenario is 992.32 tons, representing a 5.7% reduction compared to the case without hull cleaning. Hence, the optimal and most efficient hull cleaning schedule is identified as cleaning in month 18.

TABLE 9.
FUEL CONSUMPTION DIFFERENCE IN CLEANING SCENARIOS IN MONTHS 12, 18, AND 24 AT A SPEED OF 10 KNOTS

Clean		Uncleaned		Difference (ton)	
Total Added Fuel Consumption (ton)	Total Fuel Consumption (ton)	Total Added Fuel Consumption (ton)	Total Fuel Consumption (ton)		
		Cleaning in the 12th month			
10.07	959.58	26.56	992.32	32.74	3.4%
		Cleaning in the 18th month			
3.96	937.40	26.56	992.32	54.93	5.7%
		Cleaning in the 24th month			
26.56	992.32	26.56	992.32	0.00	0%

2. Hull Cleaning Time Scenario and Additional Fuel Consumption at 12 Knots

Table 10. presents the three scenarios at 12 knots. The results indicate that the minimum fuel consumption is achieved when hull cleaning is performed in month 18, with a total additional fuel consumption of 20.56 tons over 24 months. The cumulative fuel consumption for this scenario is 59.65 tons, which is 3.3% lower than that of a hull that is not cleaned. Therefore, the most efficient hull cleaning schedule is identified as hull cleaning conducted in month 18.

TABLE 10.
FUEL CONSUMPTION DIFFERENCE IN CLEANING SCENARIOS IN MONTHS 12, 18, AND 24 AT A SPEED OF 12 KNOTS

Clean		Uncleaned		Difference (ton)	
Total Added Fuel Consumption (ton)	Total Fuel Consumption (ton)	Total Added Fuel Consumption (ton)	Total Fuel Consumption (ton)		
		Cleaning in the 12th month			
9.17	1809.74	20.56	1849.18	39.44	2.2%
		Cleaning in the 18th month			
3.61	1789.54	20.56	1849.18	59.65	3.3%
		Cleaning in the 24th month			
20.56	1849.18	20.56	1849.18	0.00	0%

3. Hull Cleaning Time Scenario and Additional Fuel Consumption at 14 Knots

Table 11 presents the three scenarios at 14 knots. The results indicate that the lowest fuel consumption is achieved when hull cleaning is performed in month 18, with a total additional fuel consumption of 47.23 tons over 24 months. The cumulative fuel consumption in this scenario reaches 3,713.63 tons, which is 2.7% lower than that of a hull that is not cleaned. Therefore, the most efficient hull cleaning schedule is identified as hull cleaning conducted in month 18.

TABLE 11.
FUEL CONSUMPTION DIFFERENCE IN CLEANING SCENARIOS IN MONTHS 12, 18, AND 24 AT A SPEED OF 14 KNOTS

Clean		Uncleaned		Difference (ton)	
Total Added Fuel Consumption (ton)	Total Fuel Consumption (ton)	Total Added Fuel Consumption (ton)	Total Fuel Consumption (ton)		
		Cleaning in the 12th month			
21.07	3747.55	47.23	3815.39	67.84	1.8%
		Cleaning in the 18th month			
8.29	3713.63	47.23	3815.39	101.76	2.7%
		Cleaning in the 24th month			
47.23	3815.39	47.23	3815.39	0.00	0%

4. Hull Cleaning Time Scenario and Additional Fuel Consumption at 16 Knots

Table 12 presents the three scenarios at 16 knots. The results indicate that the minimum fuel consumption is achieved when hull cleaning is performed in month 18, with a total additional fuel consumption of 660.58 tons over 24 months. The cumulative fuel consumption in this scenario reaches 14,627.17 tons, which is 9.3% lower than that of a hull that is not cleaned. Therefore, the most efficient hull cleaning schedule is identified as hull cleaning conducted in month 18.

TABLE 12.
FUEL CONSUMPTION DIFFERENCE IN CLEANING SCENARIOS IN MONTHS 12, 18, AND 24 AT A SPEED OF 16 KNOTS

Clean		Uncleaned		Difference (ton)	
Total Added Fuel Consumption (ton)	Total Fuel Consumption (ton)	Total Added Fuel Consumption (ton)	Total Fuel Consumption (ton)		
		Cleaning in the 12th month			
294.75	15480.48	660.58	16048.38	567.90	3.6%
		Cleaning in the 18th month			
115.96	14627.17	660.58	16048.38	1421.21	9.3%
		Cleaning in the 24th month			
660.58	16048.38	660.58	16048.38	0.00	0%

IV. CONCLUSION

Based on the analysis and discussion, the biofouling growth rate is estimated at 2–3% per month. The most efficient interval for underwater hull cleaning was found to be 18 months after paint application. Analysis of the underwater hull cleaning scenario shows that cleaning at 18 months results in the lowest fuel consumption across all tested speed variations. At a speed of 10 knots, the reduction in fuel consumption reaches 5.7% or 54.93 tons, at a speed of 12 knots, the reduction in fuel consumption reaches 3.3% or 59.65 tons, at a speed of 14 knots, the reduction in fuel consumption reached 2.7% or 101.76 tons, and at a speed of 16 knots, the reduction in fuel consumption reached 9.3% or 1,421.21 tons compared to ships without hull cleaning.

ACKNOWLEDGEMENTS

The author would like to thank all individuals and institutions who indirectly supported this research through access to data, facilities, and academic feedback.

REFERENCES

[1] Demirel, Y. K., Uzun, D., Zhang, Y., Fang, H. C., Day, A. H., & Turan, O. (2017). Effect of barnacle fouling on ship resistance and powering. Biofouling, 33(10), 819–834. https://doi.org/10.1080/08927014.2017.1373279.

[2] Egan, S. (2001). Production and regulation of fouling inhibitory compounds by the marine bacterium Pseudoalteromonas tunicata.

[3] Al-Muhanna, K., & Habib, K. (2016). Marine bio-fouling of different alloys exposed to continuous flowing fresh seawater by electrochemical impedance spectroscopy. Journal of Saudi Chemical Society, 20(4), 391–396. https://doi.org/10.1016/j.jscs.2012.07.008.

[4] Demirel, Y. K., Turan, O., & Incecik, A. (2017). Predicting the effect of biofouling on ship resistance using CFD. Applied Ocean Research, 62, 100–118. https://doi.org/10.1016/j.apor.2016.12.003.

[5] Bertram, V. (2012). Practical Ship Hydrodynamics. Practical Ship Hydrodynamics. https://doi.org/10.1016/C2010-0-68326-X.

[6] Baital, Mum. S. (2016). Analisa Pengaruh Penempelan Marine Biofouling Terhadap Power Kapal Dengan Simulasi CFD.

[7] Callow, J. A., & Callow, M. E. (2011). Trends in the development of environmentally friendly fouling-resistant marine coatings. In Nature Communications (Vol. 2, Issue 1). https://doi.org/10.1038/ncomms1251.

[8] Uzun, D., Demirel, Y. K., Coraddu, A., & Turan, O. (2019). Time-dependent biofouling growth model for predicting the effects of biofouling on ship resistance and powering. Ocean Engineering, 191(June),106432.https://doi.org/10.1016/j.oceaneng.2019.106432

[9] Naval Sea Systems Command. (2006). Waterborne underwater hull cleaning of navy ships. Naval Ships' Technical Manual, 68pp.

[10] Kim, D. H., Alayande, A. B., Lee, J. M., Jang, J. H., Jo, S. M., Jae, M. R., Yang, E., & Chae, K. J. (2024). Emerging marine environmental pollution and ecosystem disturbance in ship hull cleaning for biofouling removal. In Science of the Total Environment (Vol. 906). Elsevier B.V. https://doi.org/10.1016/j.scitotenv.2023.167459.

[11] Zhong, X., Dong, J., Liu, M., Meng, R., Li, S., & Pan, X. (2022). Experimental study on ship fouling cleaning by ultrasonic-enhanced submerged cavitation jet: A preliminary study. Ocean Engineering, 258. https://doi.org/10.1016/j.oceaneng.2022.111844.

[12] Pribadi, Singgih. (2022). Studi Eksperimen Pertumbuhan Biofouling Terhadap Spesimen Uji yang Tidak Bergerak. ITS Surabaya.

[13] Wang, H., & Zhai, Z. J. (2012). Analyzing grid independency and numerical viscosity of computational fluid dynamics for indoor environment applications. Building and Environment, 52, 107–118. https://doi.org/10.1016/j.buildenv.2011.12.019

[14] Menter, F. R. (1994). Two-Equation Eddy-Viscosity Turbulence Models for Engineering Applications. 32(8).

[15] Bardina, J. E., Huang, P. G., & Coakley, T. J. (1997). TURBULENCE MODELING VALIDATION.

[16] Davanipour, M., Javanmardi, H., & Goodarzi, N. (2018). Chaotic Self-Tuning PID Controller Based on Fuzzy Wavelet Neural Network Model. Iranian Journal of Science and Technology, Transactions of Electrical Engineering, 1(2015). https://doi.org/10.1007/s40998-018-0069-1.

[17] Elhadad, A. M., El-Ela, A. M. A., & Hussien, M. M. (2023). Matlab Implementation using Holtrop and Mennen Method of Bare Hull Resistance Prediction for Surface Combatant Ship Coupled with CFD. CFD Letters, 15(10), 1–11. https://doi.org/10.37934/cfdl.15.10.111

[18] Queutey, P., & Visonneau, M. (2007). An interface capturing method for free-surface hydrodynamic flows. 36, 1481–1510. https://doi.org/10.1016/j.compfluid.2006.11.007

[19] Li, Z., Deng, G., Queutey, P., Bouscasse, B., Ducrozet, G., Gentaz, L., Touz, D. Le, & Ferrant, P. (2019). Comparison of wave modeling methods in CFD solvers for ocean engineering applications.188(June).https://doi.org/10.1016/j.oceaneng.2019.106237.

[20] Wackers, J., Koren, B., Raven, H. C., van der Ploeg, A., Starke, A. R., Deng, G. B., Queutey, P., Visonneau, M., Hino, T., & Ohashi, K. (2011). Free-Surface Viscous Flow Solution Methods for Ship Hydrodynamics. Archives of Computational Methods in Engineering, 18(1), 1–41. https://doi.org/10.1007/s11831-011-9059-4.

[21] Guilmineau, E., Deng, G. B., & Wackers, J. (2011). Numerical simulation with a DES approach for automotive flows. Journal of Fluids and Structures, 27(5–6), 807–816. https://doi.org/10.1016/j.jfluidstructs.2011.03.010

[22] Ferziger, J. H., Perić, M., & Street, R. L. (2020). Introduction to Numerical Methods BT - Computational Methods for Fluid Dynamics (pp. 23–40). https://doi.org/10.1007/978-3-319-99693-6_2.

[23] Versteeg, H. K., & Malalasekera, W. (n.d.). An Introduction to Computational Fluid Dynamics Second Edition. www.pearsoned.co.uk/versteeg.

[24] J.C.Date and S.R. Turnock (1999).G. O. A study into the techniques needed to accurately predict skin friction using RANS solvers with validation against Froude's historical flat plate experimental data Date and Turnock 1999.

[25] Chiroșcă, A. M., & Rusu, L. (2021). Comparison between model test and three CFD studies for a benchmark container ship. Journal of Marine Science and Engineering, 9(1), 1–16. https://doi.org/10.3390/jmse9010062